IEEE Photonics Journal
An IEEE Photonics Society Publication

Open Access

# Image Dehazing Based on Accurate Estimation of Transmission in the Atmospheric Scattering Model

Volume 9, Number 4, August 2017

Guoling Bi
Jianyue Ren
Tianjiao Fu
Ting Nie
Changzheng Chen
Nan Zhang

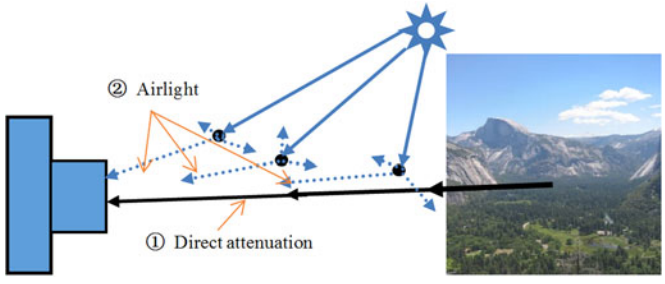


The schematic of haze image degradation

DOI: 10.1109/JPHOT.2017.2726107
1943-0655 © 2017 IEEE

IEEE photonics SOCIETY

IEEE

# Image Dehazing Based on Accurate Estimation of Transmission in the Atmospheric Scattering Model

**Guoling Bi,[1] Jianyue Ren,[1] Tianjiao Fu,[1] Ting Nie,[1] Changzheng Chen,[1] and Nan Zhang[2]**

[1]Changchun Institute of Optics, Fine Mechanics and Physics, Chinese Academy of Sciences, Changchun 130033, China
[2]Changchun Observatory, National Astronomical Observatories, Chinese Academy of Sciences, Changchun 130117, China

*DOI:10.1109/JPHOT.2017.2726107*
*1943-0655 © 2017 IEEE. IEEE. Translations and content mining are permitted for academic research only. Personal use is also permitted, but republication/redistribution requires IEEE permission. See http://www.ieee.org/publications_standards/publications/rights/index.html for more information.*

Manuscript received May 6, 2017; revised July 6, 2017; accepted July 8, 2017. Date of publication July 13, 2017; date of current version July 24, 2017. This work was supported in part by the National Natural Science Foundation of China under Grant 11403064, and in part by the Science and Technology Development Program of Jilin under Grant 20170204029GX. Corresponding author: G. Bi (e-mail: bigl_ciomp@163.com).

**Abstract:** Image dehazing is a challenging and highly desired technology in computer vision applications. The dark channel prior (DCP) has been considered to be an efficient dehazing technique in recent years. However, the invalidation of DCP can induce unreliable estimation of transmission, resulting in inaccurate color information recovery, halo artifacts, and block effect. In this paper, a novel brightness map is proposed based on the observation on outdoor haze-free/haze images that can reflect the brightness information and the light reflection ability of the scene, furthermore, the relationship between DCP and the brightness map is given in mathematical model. The proposed algorithm can compensate for the DCP effectively, estimate the transmission map accurately, get the global atmospheric light adaptively and segment the image automatically. Using multiscale guided filter refine transmission map, the halo artifacts are able to be avoided in the scene depth of a sudden change. A series of experiments are additionally implemented to demonstrate that the proposed algorithm can obtain high-quality haze-free images with abundant distinguished details, low color distortion, and little halo artifacts that can outperform or be comparable with four state-of-the-art haze removal algorithms.

**Index Terms:** Image dehazing, brightness map, transmission estimate, dark channel prior.

## 1. Introduction

When taking pictures by camera under the haze-condition, the captured images always suffer from poor visibility, low contrast and dimmed color. This is due to the atmospheric absorption and scattering. The irradiance received by the camera from the scene is attenuated along the line of sight. Furthermore, the incoming light is blended with the airlight because ambient light can be scattered into the line of sight by atmospheric particles [1]. That not only influences the visual effect, but also limits the utility of outdoor vision systems, such as object recognition and tracking, scene classification and analysis, and image segmentation [2]–[4].

Image dehazing is a challenging and highly desired technology in computer vision applications. The traditional nonphysical model algorithms include histogram equalization and its variations [5], [6], which have been the most widespread nonphysical model algorithms. Retinex [7]–[10] enhanced

image contrast in accordance with the specific needs but without showing the mechanism of image degradation. The advantages of those nonphysical model algorithms are simple but the processing results have not been satisfactory. Some improved results were also obtained employing physical-based models, which was able to analyze the image degradation mechanism by building the model to realize the scene reconstruction. In recent years, some common model of image dehazing algorithms have been proposed base on additional prior knowledge or multiple hazy images as input [11]–[18]. In depth-based methods [11]–[13], it was required to provide some depth information from user inputs or known 3D models for image dehazing. Moreover, polarization-based methods [14]–[18] were proposed to remove the haze effects through two or more images which were with different degrees of polarization. Nevertheless, taking multiple input images of the same scene is usually impractical in lots of real applications.

More recently, significant progresses have been made to remove haze from single image [19]–[25]. Tan [19] assumed that a haze-free image has a higher contrast than the hazy image. Tan maximized the contrast of a hazy image, however, the result of Tan's algorithm tended to over-compensate for the reduced contrast, yielding halo artifacts. Fattal [20] assessed the transmission map assuming that the albedo of the objects and the transmission were statistically uncorrelated. This method was able to not only restore impressive haze-free images but also provide a reliable transmission estimation of a haze scene. However, this method might fail to recover a haze-free image when the assumptions were broken. Tarel and Hautiere [21] proposed a novel algorithm for visibility restoration based on median filter in order to preserve both edges and corners. It was very fast since its complexity was only a linear function of the number of input image pixels, and it was able to achieve equally and sometime even better results to both color and gray level images. Kim *et al*. [22] formulated a cost function that consisted of the contrast term and the information loss term. By minimizing the cost function, the proposed algorithm enhanced the contrast and preserves the information optimally. A restoration algorithm [23] for weather degraded images based on the response ratio constancy of the sensors of a RGB camera effectively improved the visibility, contrast, and color in the images with no prior information about the image content and with low computational time. He *et al.* [24] proposed the famous Dark Channel Prior (DCP) to remove haze from a single image, where the key observation was that most local patches in outdoor haze-free images contained some pixels whose intensity was very low in at least one color channel. This method was able to achieve quite compelling haze-free images but it was time-consuming due to the adoption of soft matting strategy. In order to accelerate the algorithm, they further proposed an excellent edge-preserving smoothing operator named guided filter [25] which was able to avoid gradient reversal artifacts near the strong edges. With the guided filter, the quality of haze-free result was comparable to that of soft matting. However, when the scene objects were inherently similar to the atmospheric light and no shadow was cast on them, the dark channel prior will fail. Up to now, a lot of single image dehazing algorithms have been proposed based on DCP [26]–[31].

In light of the above analysis, we propose a novel single image dehazing algorithm based on accurate estimation of transmission in the atmospheric scattering model. The main contributions consist of the following aspects:

1) A novel brightness map is proposed based on observation on outdoor haze-free/haze images which can reflect the brightness information and the light reflection ability of the scene. We also gives the relationship between DCP and The brightness map in mathematical model.
2) Using a certain fusion strategy, the brightness map can effectively compensate for the DCP to estimate the transmission map accurately and get the global atmospheric light adaptively, which can effectively avoid color distortion, halo artifacts and block effect of the haze removal image.
3) When the DCP is invalid, the scene objects (such as the sky area) can be segmented automatically, which are inherently similar to the atmospheric light and no shadow is cast on them.
4) Using multi-scale guided filter refine the transmission map, which can effectively avoid the halo artifacts in the scene depth of a sudden change.

The remainder of this paper is arranged as follows. In Section 2, we review the classical dichromatic atmospheric scattering model of haze scene and discuss the advantages of DCP. In Section 3,

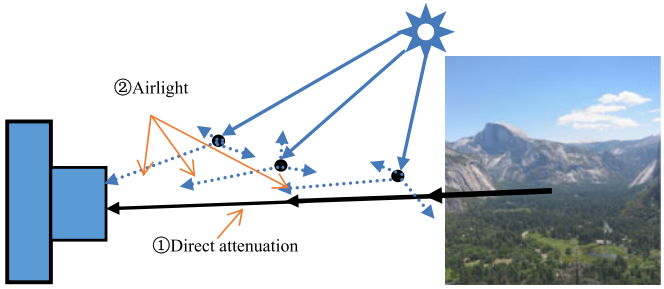


Fig. 1. The schematic of haze image degradation.

the proposed algorithm is introduced. In Section 4, we give experimental results and related discussions. Finally, we conclude this paper in Section 5.

## 2. Related Works

### 2.1 Haze Image Degradation Model

In computer vision community, the dichromatic atmospheric scattering model is widely used to describe the formation of a hazy image *I(x)*, where *x* is the pixel index, the model is usually depicted as [19], [20], [24], [32]

$$I(x) = \underbrace{J(x)t(x)}_{\text{direct attenuation}} + \underbrace{A(1-t(x))}_{\text{airlight}} \tag{1}$$

Where this equation is defined on the three RGB color channels. *I(x)* is the observed intensity, *J(x)* is the scene radiance, A is the global atmospheric light, and *t(x)* is the medium transmission indicating the portion of the light that is not scattered and reaches the camera. The schematic of haze image degradation is shown in Fig. 1.

The first item is called direct attenuation that describes the scene radiance and its decay in the medium. The second item is called airlight which results from previously scattered light and leads to the shift of the scene color. While the direct attenuation is a multiplicative distortion of the scene radiance, the airlight is an additive one. The main task of single image dehazing is to recover a haze-free image *J(x)*, A, and *t(x)* from the received image *I(x)*, which is an under-constrained problem. When the atmosphere is homogenous, in [19], [20], [24], [32], [34], they assume that the transmission *t(x)* do not change with the wavelength of light.

### 2.2 DCP Scheme

The DCP is based on the following observation on outdoor haze-free images: in most of the non-sky patches, at least one color channel has some pixels whose intensity is very low and close to zero. Equivalently, the minimum intensity in such a patch is close to zero. For an arbitrary image *J*, its dark channel $J^{\text{dark}}$ is given by

$$J^{\text{dark}}(x) = \min_{y \in \Omega(x)} \left( \min_{c \in \{r,g,b\}} J^c(y) \right) \tag{2}$$

Where *Jc* is a color channel of *J* and $\Omega(x)$ is a local patch centered at *x*. According to the concept of DCP, the intensity of dark channel of *J* is low and tends to be zero where *J* is an outdoor haze-free image, except the bright region

$$J^{\text{dark}}(x) \to 0 \tag{3}$$

He [24] proposed to use the dark channel to detect the most haze-opaque region and improve the atmospheric light estimation. They first picked the top 0.1 percent brightest pixels in the dark

channel. Among these pixels, the pixels with highest intensity in the input image were selected as the atmospheric light A. After estimating A, based on the haze imaging model shown in (1) and the DCP shown in (2) and (3), here we consider as an estimation of the transmission map *t(x)* which can be derived as

$$\tilde{t}_D(x) = 1 - \omega_D \min_{y \in \Omega(x)} \left( \min_c \frac{I^c(y)}{A^c} \right) \tag{4}$$

If the haze is removed thoroughly, the image may seem unnatural, so a constant parameter $\omega_D$ ($0 < \omega_D < 1$) is introduced to calculate the estimation of transmission $\tilde{t}_D(x)$ in (4). We fix $\omega_D$ to 0.95 for all results reported in this paper. Then, $\tilde{t}_D(x)$ is refined by the soft matting [35]. The final scene radiance $J(x)$ is recovered by

$$J(x) = \frac{I(x) - A}{\max(t_D(x), t_0)} + A \tag{5}$$

Where $t_0$ is a user-defined lower bound of $\tilde{t}_D(x)$, and a typical value of $t_0$ is 0.1.

## 3. Proposed Algorithm

In this section, we present the proposed single image dehazing algorithm. In Section 3.1 the brightness map is proposed which reflect the brightness information and the light reflection ability of the haze-free/haze scene. We also give the relationship between the brightness map and the DCP in mathematical model, In Section 3.2, using a certain fusion strategy we get an accurate transmission map according to the brightness map and the DCP. We refine the transmission map by multi-scale guided filter and get adaptive atmospheric light in Section 3.3. Finally, after recovering the scene radiance and an improved UM algorithm is used to improve the image contrast. The details of the proposed single image dehazing method are elaborated in the following subsections.

### *3.1 Brightness Map*

When the scene objects are inherently similar to the atmospheric light and no shadow is cast on them, the DCP is invalid, which may induce unreliable estimation of the transmission, resulting in inaccurate color information recovery, halo artifacts and block effect. In order to solve this problem, we conduct the following research.

We observe that most outdoor haze-free/haze images with local regions, at least one color channel has some pixels whose intensity is relatively high that represents the light intensity and the ability to reflect the light of the local regions. In this way, we get a novel map which is called “the brightness map”. For an arbitrary haze-free image J, the brightness map $J^{\text{bright}}(x)$ is shown:

$$J^{\text{bright}}(x) = \max_{y \in \Omega(x)} \left( \max_{c \in \{r,g,b\}} J^c(y) \right) \tag{6}$$

Although we have observed a large number of outdoor haze-free images, only five images are presented here to show the contrast between the dark channel images and the brightness maps, as shown in Fig. 2. As in [24], shadows and any dark object with low reflectance in any color channel, e.g., the shadows of buildings, leaves, trees, and rocks in landscape images, or dark tree trunks and stones, the DCP is effective, but the intensity of brightness map is low. On the other hand, we find the high intensity of the brightness map is mainly due to two factors: a) bright colorful objects or surfaces, e.g., white snow, white clouds and colorful flowers; b) grey objects or surfaces, e.g., white or grey buildings, grey or pale blue sky, etc. However, the DCP is invalid in those situations. Therefore, we can take a strategy to compensate for the DCP by using the brightness map.

The brightness map of haze images can also reflect the brightness information and the light reflection ability of haze scenes. For an arbitrary haze image *I*, the brightness map $I^{\text{bright}}(x)$ is shown:

$$I^{\text{bright}}(x) = \max_{y \in \Omega(x)} \left( \max_c I^c(x) \right) \tag{7}$$

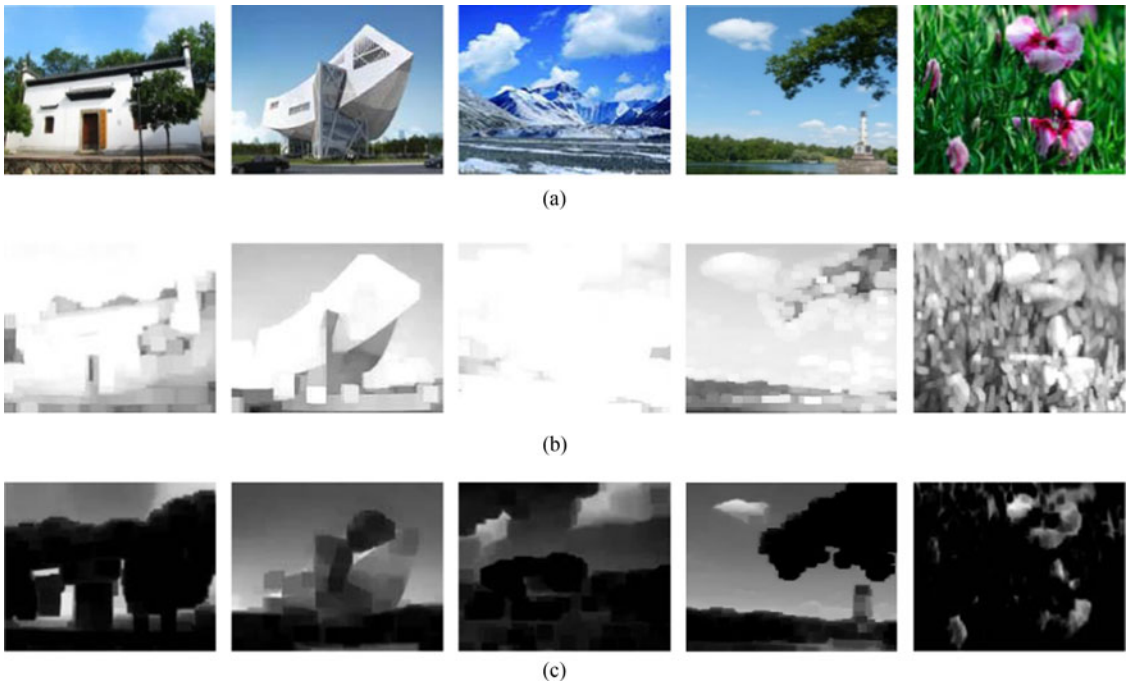


Fig. 2. The brightness maps and dark channels of haze-free images: (a) haze-free images; (b) the brightness maps, and the patch size of $\Omega$ is 15 $\times$ 15; (c) the corresponding dark channels, and the patch size of $\Omega$ is 15 $\times$ 15.

We do large numbers of experiments on haze images according to (7) and here we only select four haze images as shown in Fig. 3, the haze concentration increases from left to right.

It can be seen that the brightness map of the haze image has a high value in a large sky area with dense haze, and bright color objects, e.g., colorful flowers and white cars. So the above inference is correct: the brightness map of haze image can also reflect the brightness information and the light reflection ability of the haze scene.

Therefore, in this paper, we will use the brightness map to guide and compensate for the DCP to obtain accurate transmission map which can effectively avoid the errors of dark channel. In order to highlight the guiding role of the brightness map, we take a linear stretch to enhance the contrast of the brightness map. Get the rough estimation of the brightness map as (8) shows:

$$\tilde{I}_B(x) = \frac{I^{\text{bright}}(x) - \min(I^{\text{bright}}(x))}{\max(I^{\text{bright}}(x)) - \min(I^{\text{bright}}(x))} \tag{8}$$

Where $\max(I^{\text{bright}}(x))$ is the maximum value of haze image $I^{\text{bright}}(x)$, $\min(I^{\text{bright}}(x))$ is the minimum value of haze image $I^{\text{bright}}(x)$.

It can be seen from (4) that the transmission map $\tilde{t}_D(x)$ is a decreasing function of $\min_{y\in\Omega(x)}(\min_c I^c(x))$, indicating that the smaller of $\min_{y\in\Omega(x)}(\min_c I^c(x))$, the larger of the transmission map $\tilde{t}_D(x)$, the greater probability that the local image (for example, the shadows of leaves, trees) is in line with the DCP. On the other hand, the larger of $\min_{y\in\Omega(x)}(\min_c I^c(x))$, the smaller of the transmission map $\tilde{t}_D(x)$, the smaller probability that the local image(for example, grey or pale blue sky) is in line with the DCP.

It can be seen from (8) that the brightness map $\tilde{I}_B(x)$ is an increasing function of $I^{\text{bright}}(x)$, indicating that the smaller of $I^{\text{bright}}(x)$, the smaller of the brightness map $\tilde{I}_B(x)$, the greater probability that the local image (for example, the shadows of leaves, trees) is in line with the DCP. On the other hand, the larger of $I^{\text{bright}}(x)$, the larger of the brightness map $\tilde{I}_B(x)$, the smaller probability that the local image (for example, grey or pale blue sky) is in line with the DCP.

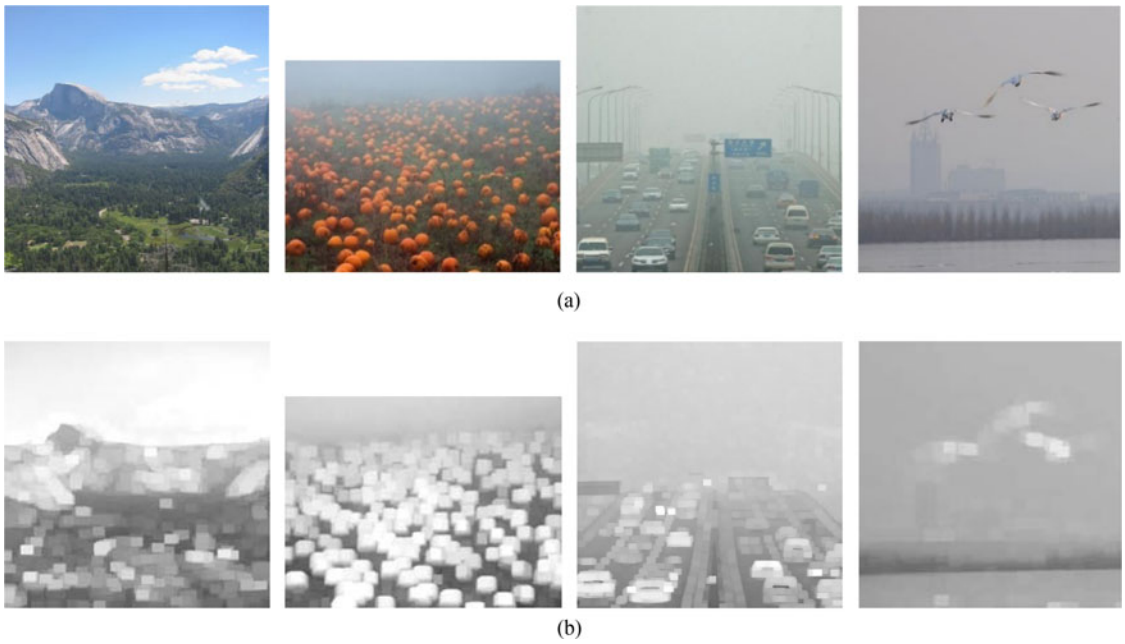


Fig. 3. The brightness maps of haze images: (a) the arbitrary haze images; (b) the brightness maps, and the local size of $\Omega(x)$ is 15 $\times$ 15.

In conclusion, the local images (for example, grey or pale blue sky) have the smaller probability in line with the DCP while often have larger value of the brightness map $\tilde{I}_B(x)$. Therefore, the estimation of brightness map can compensate for the DCP to estimate the transmission map more accurately. In the next section, we propose a strategy to fuse of the brightness map and the transmission map.

### *3.2 Accurate Estimation of the Transmission*

Here, we select one haze image with sky regions for simulation experiments. According to the method of He [24], we first pick the top 0.1 percent brightest pixels in the dark channel. Among these pixels, the pixels with highest intensity in the input image are selected as a rough estimation of the atmospheric light A. We get a rough estimation of the transmission map $\tilde{t}_D(x)$ according to (4) and get the estimation of brightness map $\tilde{I}_B(x)$ according to (8), the results are shown in Fig. 4(b) and (c), respectively.

By the analysis of Section 3.1, according to the rough estimation of transmission map $\tilde{t}_D(x)$ and brightness map $\tilde{I}_B(x)$, determine the probability of local pixel values that conform to the DCP, we adopt the strategy of (9). In this way, the brightness map can effectively compensate for the DCP when the DCP is invalid, and ultimately to obtain more accurate estimation of the transmission $\tilde{t}_E(x)$.

If $\tilde{t}_D(x) \geq$ thD, indicating the scene radiance is usually not as bright as the atmospheric light, the local image is more in line with the DCP, then estimating of the transmission in line with the DCP.

If $\tilde{I}_B(x) \geq$ thB and $\tilde{t}_D(x) <$ thD , indicating the local image is not in line with the DCP, the scene radiance is usually as bright as the atmospheric light and the transmission is underestimated. Therefore, the estimation of the transmission should be increased. In this case, the transmission map and the brightness map have vast difference, we take a weighted average of the both maps to get an accurate estimation of the transmission map. In order to prevent the value too large, we add a disturbance constant $\delta$ and adopt $\delta = 0.1$, as shown in (9). It's worth pointing out that all of the images are first normalized and then processed in this paper.

Here, we get the value thD and thB adaptively by using histogram statistics. From the analysis of Section 3.1, For the transmission map $\tilde{t}_D(x)$, the smaller the value, the smaller probability in line

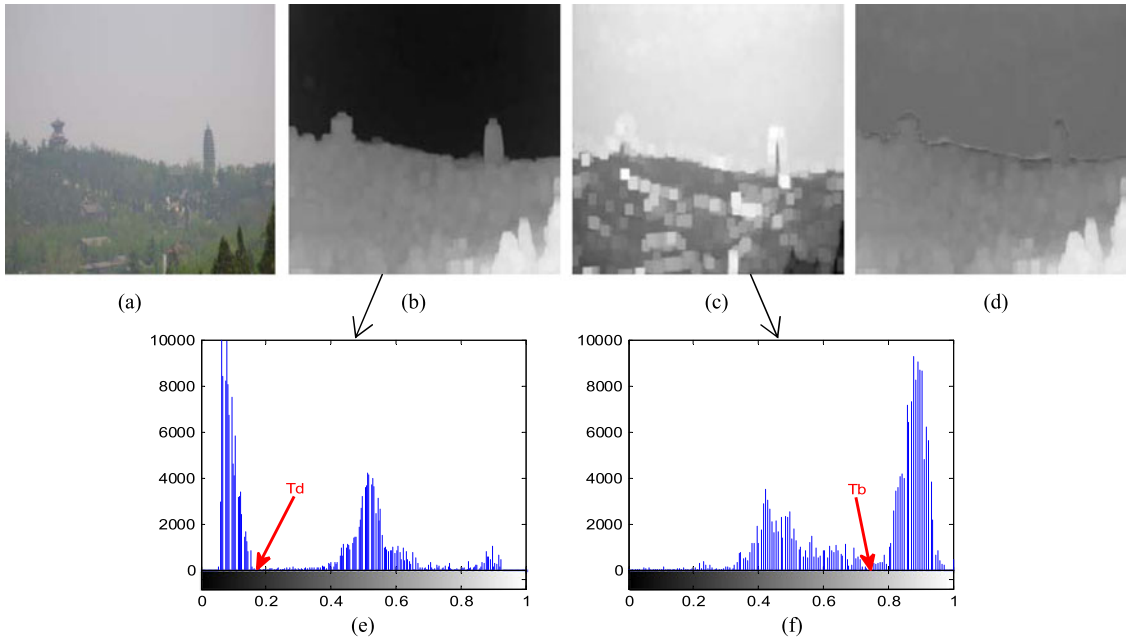


Fig. 4. Estimation of transmission of a haze image: (a) an arbitrary image; (b) the rough estimation of transmission map $\tilde{t}_D(x)$; (c) the estimation of brightness map $\tilde{I}_B(x)$; (d) a rough estimation of transmission map $\tilde{t}_E(x)$; (e) the histogram of $\tilde{t}_D(x)$; (f) the histogram of $\tilde{I}_B(x)$.

with the DCP, the statistics histogram of $\tilde{t}_D(x)$ is shown in Fig. 4(e), traversing from the minimum value 0 to the maximum 1, select the first trough value Td as the threshold of thD.

For the brightness map $\tilde{I}_B(x)$, the larger the value, the smaller probability in line with the DCP, and the statistical histogram of $\tilde{I}_B(x)$ is shown in Fig. 4(f), traversing from the maximum value 1 to the minimum value 0, select the first trough value Tb as the threshold of thB.

In other cases, in order to estimate the transition areas of the transmission map smoother, we induce the parameters of $\lambda_1(x)$ and $\lambda_2(x)$, and use a linear weight approach to get an accurate estimation of the final local transmission $\tilde{t}_E(x)$, as shown in (9). The weight relationship between the transmission map and the brightness map satisfies the (10) and the (11).

$$\tilde{t}_E(x) = \begin{cases} \tilde{t}_D(x) & \tilde{t}_D(x) \geq \text{thD} \\ (\tilde{t}_D(x) + \tilde{I}_B(x))/2 - \delta & \tilde{I}_B(x) \geq \text{thB and } \tilde{t}_D(x) < \text{thD} \\ \lambda_1(x)\tilde{t}_D(x) + \lambda_2(x)\tilde{I}_B(x) & \text{others} \end{cases} \tag{9}$$

$$\lambda_1(x) = \begin{cases} \frac{\tilde{t}_D(x)}{\tilde{t}_D(x)+\tilde{I}_B(x)} & \tilde{t}_D(x) \geq \tilde{I}_B(x) \\ \frac{\tilde{I}_B(x)}{\tilde{t}_D(x)+\tilde{I}_B(x)} & \tilde{t}_D(x) < \tilde{I}_B(x) \end{cases} \tag{10}$$

$$\lambda_2(x) = 1 - \lambda_1(x) \tag{11}$$

Here, we use the convergence strategy and use the brightness map to compensate and correct the transmission map which is estimated by the DCP. Finally we get an accurate and rough estimation of the transmission map as shown in Fig. 4(d).

### *3.3 Transmission Refinement and Estimation of Atmospheric Light*

In the above Section, we assume that all pixels in a patch have the same transmission value. However, scene depth is not always constant in a patch, which causing some halo artifacts. Therefore, an edge preserving filter that named guided filter [25] is employed to get a refined estimation of the transmission.

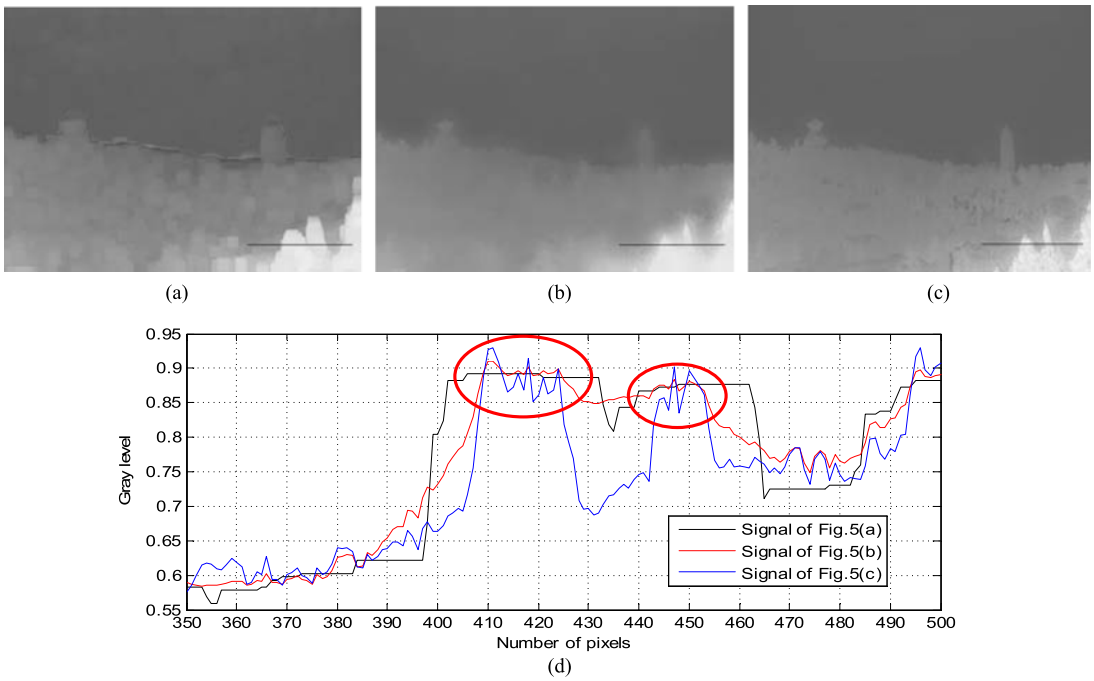


Fig. 5. The refined estimation of the transmission by the guided filter: (a) a rough estimation of transmission map; (b) a refined estimation of transmission by single scale guided filter; (c) a refined estimation of transmission by multi-scale guided filter; (d) one-dimensional signal of the 330th row of the above transmission images from column 350 to column 550.

when we refine the transmission map by the guided filter, the radius $r$ of local smooth window is bigger, guided image will get average linear output in a larger range, making the edges and details of the image be more abundant and the transition be smoother, so as to avoid the block effect and halo artifacts.

When the value of $r$ is too large, it is prone to over-saturation phenomenon. When the value of $r$ is small, the edges of the image become blurred and the sharpening effect is not obvious. So for detailed images, the guided filter based on single scale can't obtain good effect. Therefore, we adopt the multi-scale guided filter to refine the transmission map, which can separate the high frequency information, make each size of the structures and the details appear under different scales, alleviate the blocking effect, and enhance the image details.

In the paper we choose the high, medium and low three different scale factors. Get the refined estimation of the transmission at different scales $\tilde{t}_i(x, y)$, take the different scale parameter merged with the linear weight to get refined transmission $\tilde{t}_m(x, y)$ is shown in the (12).

$$\tilde{t}_m(x, y) = \sum_{i}^{n} \eta_i(\tilde{t}_i(x, y)) \tag{12}$$

Where $n$ is the number of selected scale, $\eta_i$ is the scale weight, in this paper $n = 3$, $\eta_i = \frac{1}{3}$. Through a large number of experiments, in order to get the value of $r$ adaptability, considering the guided filter using box-filter, the choice of $r$ as shown in the following formula: $r_{\min} = [\min(H, W)/(2^{(n+2)})]$, $r_{\max} = [\min(H, W)/(n+2)]$, $r_{\text{mid}} = [(r_{\max} + r_{\min})/2]$, where $H$ and $W$ is the height and width of image, $r_{\min}$, $r_{\max}$ and $r_{\text{mid}}$ is the minimum, maximum and medium of $r$ respectively, [ ] indicates truncating operation. It's also worth pointing out that there is another key regularization parameter $\varepsilon$ in the guided filter. Here, we adopt $\varepsilon = 0.01$ for all results reported in this paper.

We still use the haze image in Fig. 4 to test and refine the rough estimation of transmission map as shown in Fig. 5(a) by single scale ($r = r_{\min}$) guided filter and multi-scale guided filter, the results are shown in Fig. 5(b) and (c) respectively. In order to more intuitively show the effect, we select

one-dimensional signal of the 330 th row and the column from 350 to 550 in Fig. 5(a)–(c) which is marked by black line. The one-dimensional signals with a sudden change of the scene depth are displayed in Fig. 5(d) with black, red and blue curve respectively.

In Fig. 5(d), there are two peaks which are marked with red circles. Compare with the refined transmission map by guided filter, the peak of the rough estimation of transmission is not obvious, and the edges of the tree information are not accurate. On the other hand, Compare with the refinement of transmission map by single scale guided filter, the refinement of transmission map by multi-scale guide filter has more obvious edge gradient descent and more clear edge details of the trees (as shown by the red and blue curve from column 428 to column 442). Therefore, we see that the guided filter reduce halo artifacts more effectively and preserve image details more accurately. In addition, the multi-scale guided filter can more effectively avoid the halo artifacts in the scene depth of a sudden change and provide more faithful transmission values than the single scale guided filter.

The atmospheric light A as one of the key parameters plays an important role in image dehazing. The scene radiance is usually as bright as the atmospheric light when $\tilde{I}_B(x) \geq$ thB and $\tilde{t}_D(x) <$ thD in (9), so we calculate the average of the part with the original image as an adaptive and accurate estimation of atmospheric light $A = A_{\text{ave}}$. In Section 3.2, thB and thD are based on adaptive selection of the image histogram statistics, so that we achieve to get the atmospheric light adaptively and accurately.

### 3.4 Recovering the Scene Radiance

With the adaptive and accurate estimation of atmospheric light and the refined estimation of transmission, we can recover the scene radiance according to (1). Similar to [24], we also introduce a lower bound $t_0$ to preserve a small amount of haze in very dense haze regions ($t_0$ is also set to 0.1 based on [24]). Finally, the haze-free image *J(x)* can be derived as:

$$J(x) = \frac{I(x) - A_{ave}}{\max(\tilde{t}_m(x), t_0)} + A_{ave} \tag{13}$$

Since the scene radiance is usually not as bright as the atmospheric light, the image after haze removal looks dim [24]. We adopt UM (Unsharp Masking) algorithm to enhance the dehazing image *J(x)*. The guided filter is employed to get the low-frequency image *L(x)*, the fixed magnification $N = 2$. However, large areas of the sky appear pseudo color and halo artifacts. This is because the UM method amplifies all the high frequency information by the same multiple, not only enlarging the image detail information, but also amplifying the noise. According to the human visual characteristics, the human eye is particularly sensitive to the high frequency noise of the smooth area, so we connect the magnification of the UM algorithm with the dual channel prior, and make the flat area and other areas of high-frequency information enlarged with different magnifications, so as to amplify the useful details and suppress the noise at the same time.

In the previous discussion, in (9), the condition of $\tilde{I}_B(x) \geq$ thB and $\tilde{t}_D(x) <$ thD $\tilde{I}_B(x) \geq$ thBand$\tilde{t}_D(x) <$ thD is mainly corresponding to sky region based on the dual channel prior, the image $A_e(x)$ with sky segmentation according to (14) as shown in Fig. 6(a). We select a different magnification for different regions according to (15) and get the magnification image as shown in Fig. 6(b), where $M = 2$. But we find that there is a significant block effect in the sky areas, which will lead to uneven color of enhanced image. So we use the guided filter to smooth it, and get a more fine and smooth image of different magnifications according to different pixels, as shown in Fig. 6(c).

$$A_e(x) = \begin{cases} 0 & \tilde{t}_D(x) \geq \text{thD} \\ \tilde{t}_E(x) & \text{others} \end{cases} \tag{14}$$

$$n(x) = \begin{cases} M(e^{A_e(x)}) & \tilde{t}_D(x) \geq \text{thD} \\ e^{A_e(x)} - 1 & others \end{cases} \tag{15}$$

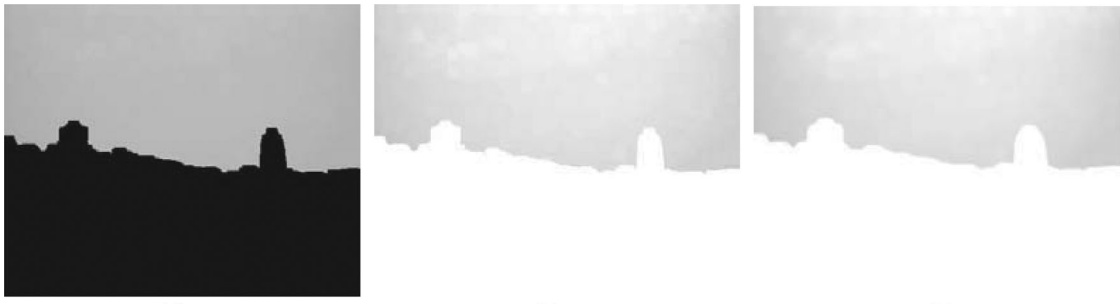

(a) (b) (c)

Fig. 6. (a) the image with sky segment; (b) the magnification image; (c) smooth (b) by the guided filter, the filter radius $r = 3$.

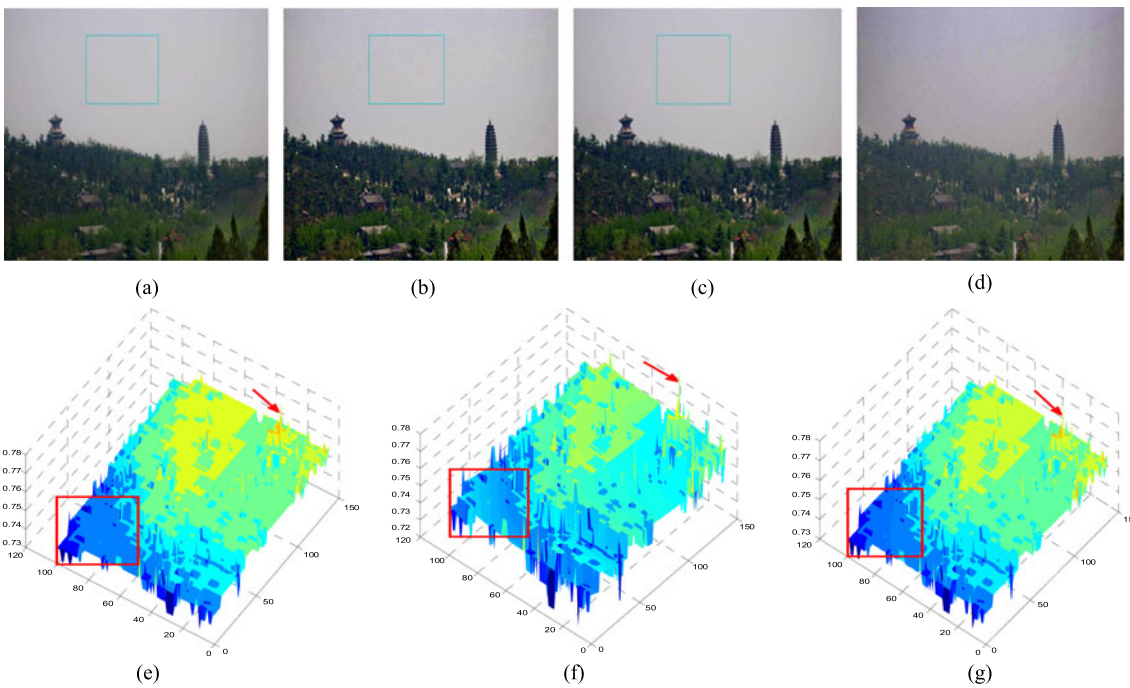

(a) (b) (c) (d)

(e) (f) (g)

Fig. 7. Scene recovering and enhancement: (a) haze removal image; (b) the UM algorithm enhanced image; (b) the improved UM algorithm enhanced image; (d) He's algorithm result; (e) three-dimensional of the local image in Fig. 7(a); (f) three-dimensional of the local image in Fig. 7(b); (g) three-dimensional of the local image in Fig. 7(c).

Finally, the result of He's algorithm [24] is shown in Fig. 7(d), the result of our dehazing algorithm is shown in Fig. 7(a), we get the enhanced image according to (16) as shown in Fig. 7(c), and get the enhanced image according to UM algorithm as shown in Fig. 7(b). The three-dimensional representation of the local image in the green boxes of Fig. 7(a)–(c) are shown in Fig. 7(e)–(g), we can see clearly from the parts of the red boxes marked, the sky part has the halo artifacts by the UM algorithm but the halo artifacts are alleviated by our improved algorithm. At the same time, as shown by the red arrows in Fig. 7(e)–(g), the individual pixels indicated by the red arrows in the Fig. 7(e) are significantly protruded which can be regarded as noise, the improved algorithm expand the dynamic range of image and improve the contrast of image without enlarge the noise.

$$J_E(x) = (J(x) - L(x))n(x) + L(x) \tag{16}$$

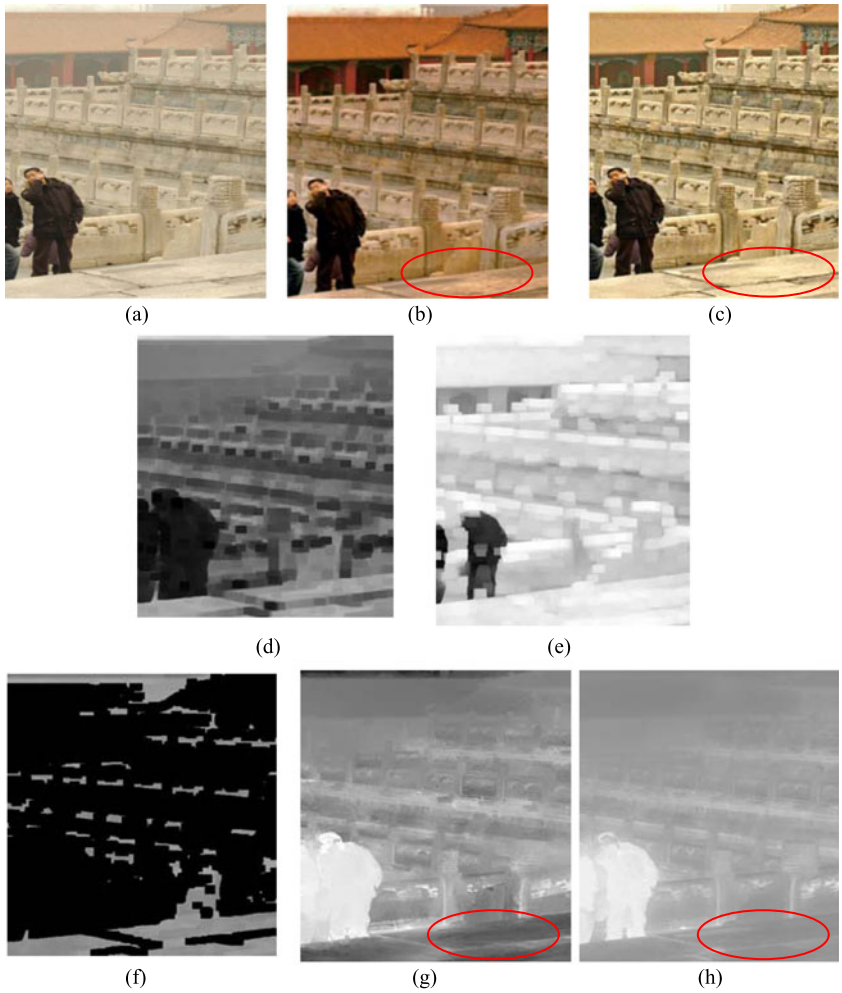


Fig. 8. Failure of the DCP: (a) input image; (b) He's result; (c) our result; (d) the dark channel of the haze image; (e) the brightness map of haze image; (f) image segmentation; (g) He's transmission map; (h) our transmission map.

## 4. Experimental Result and Analysis

### *4.1 Process the Failure of DCP*

He [24] choose two images to explain the failure of DCP, here we take the two original images from his paper for experiment as shown in Figs. 8(a) and 9(a). When the scene objects are inherently similar to the atmospheric light and no shadow is cast on them (such as the white marble in Fig. 8(a)), the DCP is invalid. The dark channel of the scene radiance has bright values near such objects as shown in Fig. 8(d). As a result, the DCP underestimate the transmission of these objects and overestimate the haze layer as shown in Fig. 8(g), especially the local image indicated by the red circle in Fig. 8. The brightness map that represents the light intensity as shown in Fig. 8(e), which can compensate for the DCP to estimate the transmission map $t(x)$ more accurately in (1).

The result of He's algorithm is shown in Fig. 8(b), the whole image lose color fidelity and slant yellow, the DCP failed. Our algorithm can get the adaptive segmentation with the local image which does not conform to the DCP according to (14) as shown in Fig. 8(f), where the gray areas indicate the DCP is invalid. The final transmission map is estimated more accurately based on the fusion of the transmission map which is estimated according to the DCP and the brightness map as shown

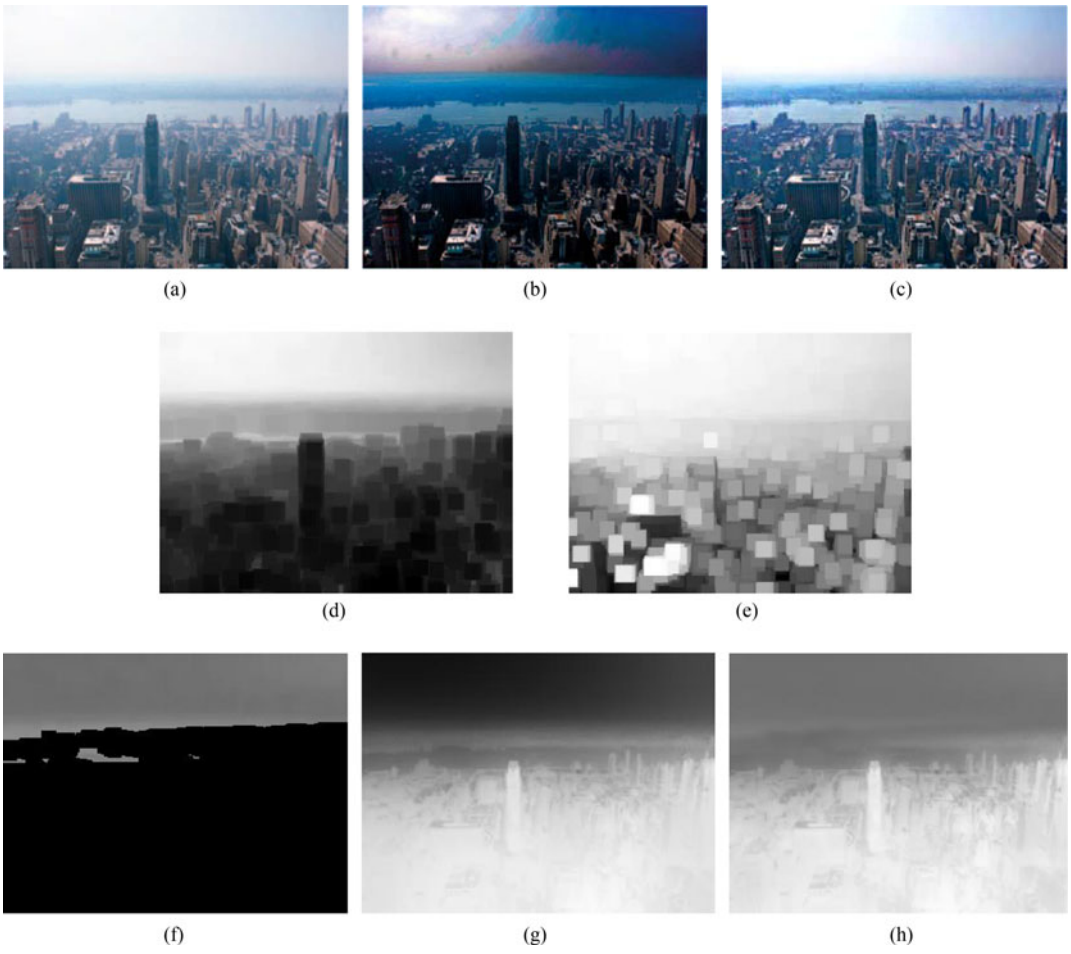


Fig. 9. Failure of the DCP: (a) input image; (b) He's result; (c) our result; (d) the dark channel of the haze image; (e) the brightness map of haze image; (f) image segmentation; (g) He's transmission map; (h) our transmission map.

in Fig. 8(h). Our method get more reliable estimation of transmission map and atmospheric light, resulting in better image recovery without sacrificing the fidelity of the color (e.g., the white marble in red circle) as shown in Fig. 8(c).

Then, we select another image to test with the sunlight is very influential, as shown in Fig. 9. When some objects are brighter than the atmospheric light where He [24] estimated the atmospheric light $A = 0.9922$, He get the estimation of transmission map only dependent on the atmospheric light $A$ and the DCP according to (4),which lead to underestimate the transmission map of the sky regions (Fig. 9(e)). The dark channel of the haze image as shown in Fig. 9(d). In Fig. 9(a), the atmospheric light is bright on the left and dim on the right, so the recovered sky region on the right is darker than it should be and the halo artifacts are also significantly in He's result as shown in Fig. 9(b).

In contrast, our algorithm adopt a certain fusion strategy according to (9), not only depend on the atmospheric light A and the DCP but also combine with the brightness map (as shown in Fig. 9(e)) represents the light intensity which prevents the invalid estimation of the transmission map *t(x)* in (1). At the same time, our algorithm can segment the local image adaptively which does not conform to the DCP according to (14) as shown in Fig. 9(d), where the gray areas indicate the DCP is invalid, estimate the atmospheric light automatically, where $A = 0.9158$, and estimate the transmission map (Fig. 9(f)) more reliably. Our algorithm achieve better color information recovery than that of He's method (Fig. 9(c)).

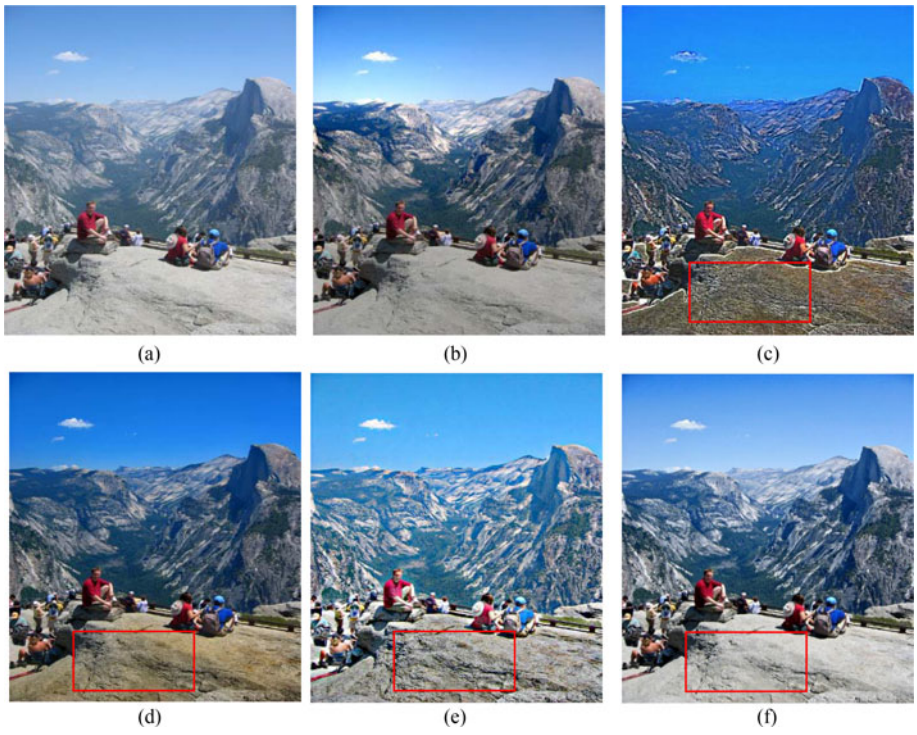


Fig. 10. Comparison with other methods: (a) input image; (b) Fattal's result; (c) Tan's result; (d) He's result; (e) Tarel's result; (f) our result.

### 4.2 Compared With Other Classical Algorithms

Here, we make the comparison of our results with four state of the art visibility restoration algorithms: Tan [19], Fattal [20], Tarel [21] and He [24], as shown in Figs. 10–12. It can be seen from Fig. 10, the result of our algorithm, Fattal's algorithm and Tarel's algorithm get natural color and high contrast, He's and Tan's algorithm although improve the contrast significantly, but the color of the image is distorted obviously, especially the sky area and close-up stone which indicated by red square area as shown in Fig. 10.

Similar observations can also be found in Fig. 11. It shows that the large area of the sky area is recovered by other algorithms with low fidelity of the color and different degrees of halo artifacts, especially the algorithm of Tan. Our algorithm recovers the sky area without sacrificing the fidelity of the color and the halo artifacts are also significantly small.

In Fig. 12, notice that the result is obtained by our algorithm seems close to the results obtained by He and Tarel, with less saturated color compared with Tan, with high contract compared with Fattal. It can be seen that there is a significant improvement in image contrast, especially at the region outline by the red rectangle in the dehazing results. The enlarged red rectangles as shown in Fig. 12(c)–(f) are more apparent. By the way, the automatic segmentation according to (14) of Figs. 10(a)–12(a) are shown in Fig. 13, where the gray areas indicate the DCP is invalid.

In addition, the proposed algorithm can also be applied to remove inhomogeneous haze and dense haze of the images. Here we select the image of inhomogeneous haze (Fig. 14(a)) from Fattal's paper and compared with Fattal's algorithm. Even if Fattal's algorithm [23] can remove the haze more completely than our method, but the sky region is too bright and the color of some tree regions are too white (Fig. 14(b)). Our algorithm employs the brightness map and DCP, which gets estimation of the transmission map more accurately and keep a very small amount of haze suitably, resulting in more natural recovery of image as shown in Fig. 14(c).

We select dense haze image as shown in Figs. 15(a) and 16(a). The results of Fattal's and He's algorithm are shown in Figs. 15(b) and 16(b), respectively. Fattal's method is based on local


Fig. 11. Comparison with other methods: (a) input image; (b) Fattal's result; (c) Tan's result; (d) He's result; (e) Tarel's result; (f) our result.

statistics and requires sufficient color information and variance. When the haze is dense, the color is faint and the variance is not high enough for his method to estimate the reliable transmission. As can be seen, our algorithm can unveil the details and recover nature color and high contrast even in heavily hazy regions as shown in Fig. 15(c), for example the regions are outlined by the red rectangle in the dehazing results. He's result in close range, the image is clear, the contrast is improved, but the sky with color distortion and block effect are also significant in depth of field. It can be seen that our algorithm can achieve a better performance both in close-range and in the distant sky(outlined by the red rectangle in the dehazing results), the details are enhanced and the contrast has been improved as shown in Fig. 16(c), thanks to the brightness map compensates for the estimation of transmission map.

### *4.3 Quantitative Evaluation*

The performance of haze removal is evaluated by calculating the mean square error (MSE) and image information entropy (IIE). The MSE and the IIE are defined as follows:

$$\mathrm{MSE} = \left[ \frac{1}{M \times N} \sum_{i=0}^{M} \sum_{j=0}^{N} (I(i,j) - \mu)^2 \right]^{1/2} \tag{17}$$

$$\mathrm{IIE} = -\sum_{r=0}^{L-1} \frac{H_r}{M \times N} \log \frac{H_r}{M \times N} \tag{18}$$

Where $M$ and $N$ represent the pixel number of the length and width of an image respectively, $I(i,j)$ is the gray value, $\mu$ is the gray mean of the image, $L$ is the maximum gray scale of the image,

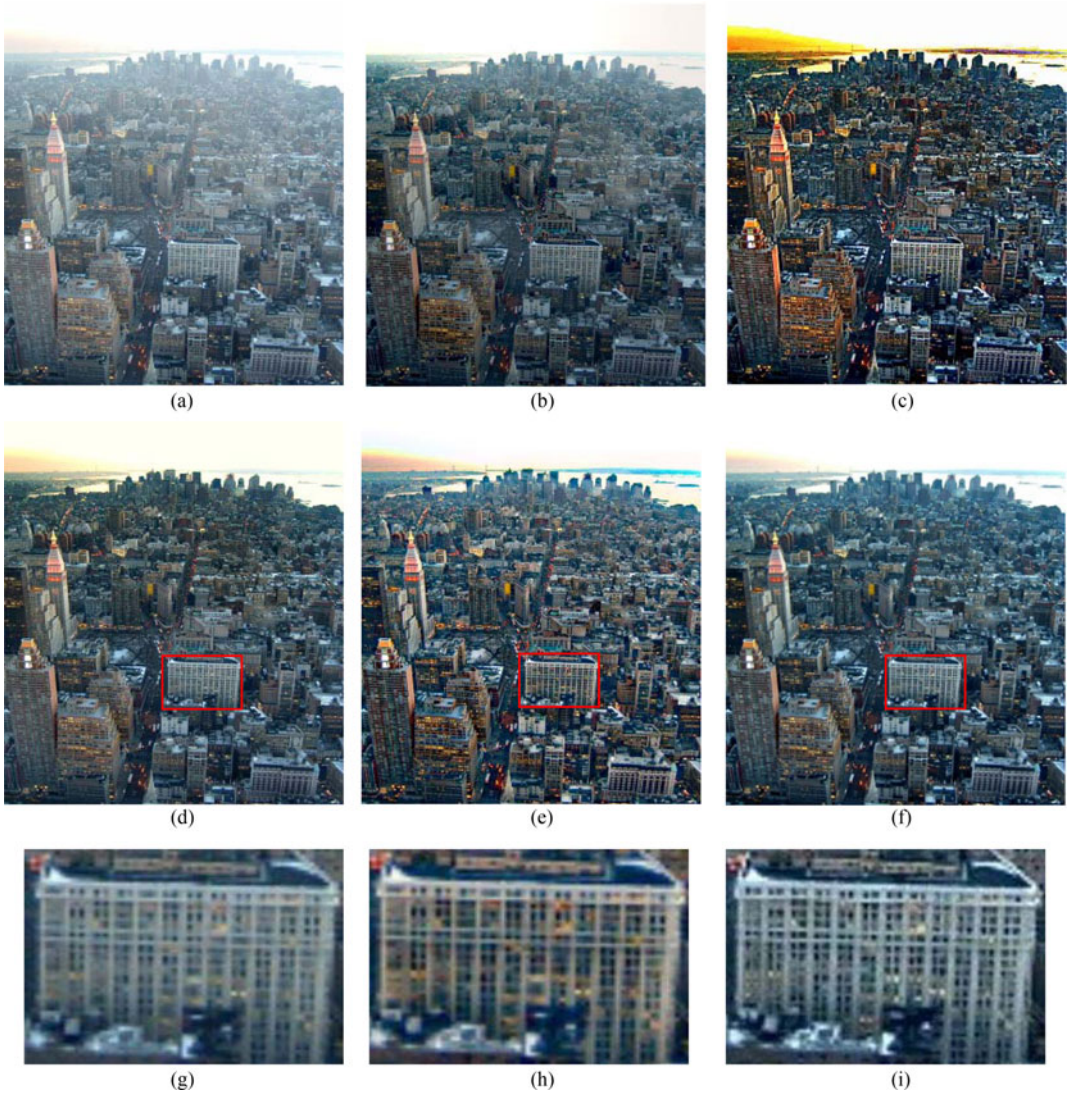


Fig. 12. Comparison with other methods: (a) input image; (b) Fattal's result; (c) Tan's result; (d) He's result; (e) Tarel's result; (f) our result.

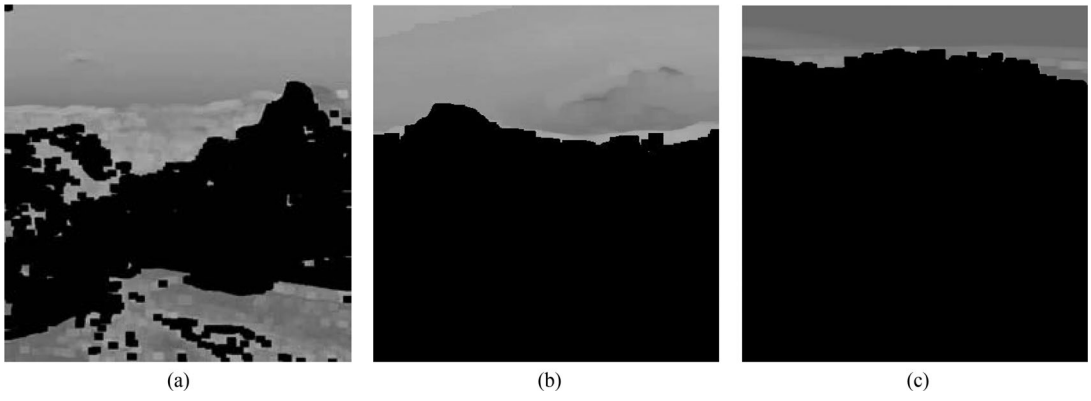


Fig. 13. Automatic image segmentation when DCP is invalid: (a) image segmentation of Fig. 10(a); (b) image segmentation of Fig. 11(a); (c) image segmentation of Fig. 12(a).


Fig. 14. The inhomogeneous haze image dehazing: (a) input image; (b) Fattal's result; (c) our result.

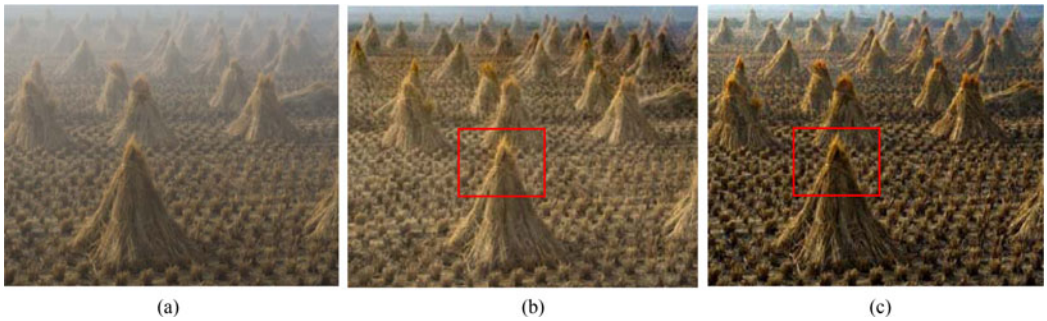


Fig. 15. The dense haze image dehazing: (a) input image; (b) Fattal's result; (c) our result.

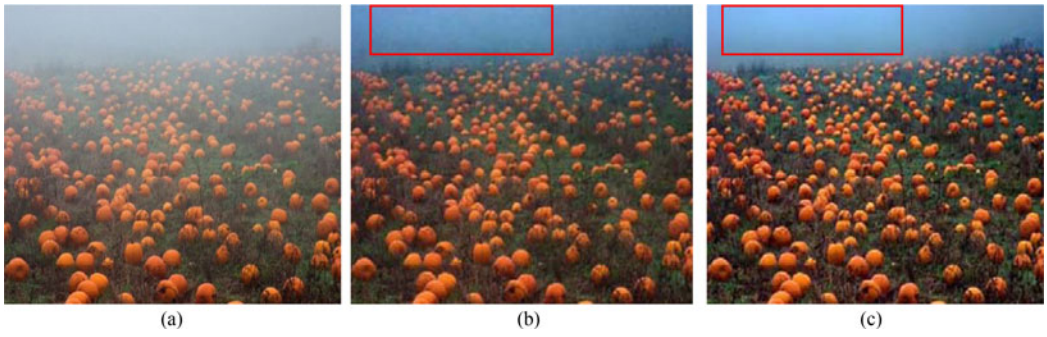


Fig. 16. The dense haze image dehazing: (a) input image; (b) He's result; (c) our result.

$H_r$ is the number of the gray level $r$ in the image, $\frac{H_r}{M \times N}$ indicates the probability that the gray level $r$ appears in the image.

If the MSE and the IIE are bigger, indicating a better performance of image dehazing algorithm which make the image details clear and contrast high. We calculate the MSE and the IIE of Figs.10–12 for objective comparison of haze removal effect by different algorithms, which are listed in Tables 1 and 2, respectively.

In Table 1, for Figs. 11 and 12, the MSE of the image dehazing by the algorithm of Tan is higher than our algorithm, this is because the algorithm of Tan has more serious overcorrection in the two images, making the image contrast higher and the MSE value larger. In Table 2, for Fig. 12, the IIE of the image dehazing by the algorithm of Tarel is higher than our algorithm, this is because the algorithm of Tarel causes the halo artifacts and color distortion in the sky region, resulting in too much useless information. It can be seen from Tables 1 and 2 that compared with the other four state of the art visibility restoration algorithms, our algorithm has obtained a higher value in the quantitative analysis of MSE and IIE, which shows that our dehazing algorithm improves the image contrast and enhances the image details effectively.

TABLE 1
Objective Comparison of Image Enhancement Effect Using MSE

| MSE | Original | He | Fattal | Tan | Tarel | Our |
|---|---|---|---|---|---|---|
| Fig. 10 | 51.7886 | 69.5700 | 61.3084 | 65.4009 | 62.4970 | 72.1100 |
| Fig. 11 | 61.0059 | 70.9711 | 67.1626 | 83.4357 | 54.8996 | 77.8436 |
| Fig. 12 | 62.6247 | 68.7489 | 72.5200 | 77.4820 | 72.9527 | 75.0718 |

TABLE 2
Objective Comparison of Image Enhancement Effect Using IIE

| IIE | Original | He | Fattal | Tan | Tarel | Our |
|---|---|---|---|---|---|---|
| Fig. 10 | 7.6291 | 7.7872 | 7.8213 | 7.7450 | 7.5049 | 7.8702 |
| Fig. 11 | 7.5897 | 7.5491 | 7.6338 | 7.4614 | 7.5873 | 7.7327 |
| Fig. 12 | 7.2473 | 7.1286 | 7.3050 | 7.2393 | 7.4658 | 7.3208 |

## 5. Conclusion

In this paper, we have proposed a novel single image dehazing algorithm based on accurate estimation of transmission in the atmospheric scattering model, where a novel brightness map is proposed based on the observation on outdoor haze-free/haze images which can reflect the brightness information and the light reflection ability of the scene, the relationship between DCP and the brightness map is given in mathematical way. According to the brightness map, we separate the DCP failure areas (such as the sky area) automatically and use a certain fusion strategy to correct the invalid estimation of the transmission map based on the brightness map and DCP, which can reduce the color distortion, block effect and halo artifacts of those areas. Since those areas are closed to the atmospheric light, so the atmospheric light can be obtained adaptively by calculating the mean value of those areas in the original haze image. Using multi-scale guided filter refine transmission map, the halo artifacts can be avoided effectively in the scene depth of a sudden change. Finally, the improved UM algorithm is used to improve the image contrast after image dehazing. Taking qualitative and quantitative comparison with the four state-of-the-art methods [19]–[21], [24], a series of experiments are additionally implemented to demonstrate the proposed algorithm can obtain high-quality haze-free images with abundant distinguished details, low color distortion and little halo artifacts which can outperform or be comparable with four state-of-the-art haze removal algorithms.

Although we use the guided filter instead of soft matting [24] to refine the transmission which can avoid the computational complexity, but the algorithm cannot meet the real-time requirement of image processing. For future work, we will extend our static image dehazing algorithm to the real-time video dehazing, which would meet the practical engineering needs.

## Acknowledgment

The authors would like to thank the reviewers for their valuable suggestions. They would also like to thanks Prof. J.-S. Zhang for proofreading final paper carefully for spelling and grammar errors.

## References


[1] S. G. Narasimhan and S. K. Nayar, "Vision and the atmosphere," *Int. J. Comput. Vis.*, vol. 48, no. 3, pp. 233–254, 2002.
[2] Y. P. Guan, "Spatio-temporal motion-based foreground segmentation and shadow suppression," *IET Comput. Vis.*, vol. 4, no. 1, pp. 50–60, 2010.
[3] M. Xu, T. Ellis, S. J. Godsill, and G. A. Jones, "Visual tracking of partially observable targets with suboptimal filtering," *IET Comput. Vis.*, vol. 5, no. 1, pp. 1–13, 2011.
[4] A. Yilmaz, "Object tracking: A survey," *ACM Comput. Surv.*, vol. 38, no. 4, 2006, Art. no. 13.
[5] J. A. Stark, "Adaptive image contrast enhancement using generalizations of histogram equalization," *IEEE Trans. Image. Process.*, vol. 9, no. 5, pp. 889–896, May 2000.
[6] H. Zhu, F. H. Y. Chan, and F. K. Lam, "Image contrast enhancement by constrained local histogram equalization," *Comput. Vis. Image. Understanding*, vol. 73, no. 2, pp. 281–290, 1999.
[7] E. H. Land, "The retinex theory of color vision," *Sci. Amer.*, vol. 237, no. 6, pp. 108–28, 1977.
[8] J. Li, "Application of image enhancement method for digital images based on retinex theory," *Optik*, vol. 124, no. 23, pp. 5986–5988, 2013.
[9] A. R. Ma, W. Wang, and S. Liu, "Extracting roads based on retinex and improved canny operator with shape criteria in vague and unevenly illuminated aerial images," *J. Appl. Remote Sens.*, vol. 6, no. 1, 2012, Art. no. 063610.
[10] M. Elad, "Retinex by two bilateral filters," in *Scale Space and PDE Methods in Computer Vision*, B. Burgeth, ed. New York, NY, USA: Springer, 2005, pp. 217–229.
[11] J. Kopf *et al.*, "Deep photo: Model-based photograph enhancement and viewing," *ACM Trans. Graph*, vol. 27, no. 5, pp. 1–10, 2008.
[12] S. G. Narasimhan and S. K. Nayar, "Interactive deweathering of an image using physical models," in *Proc. Int. Conf. IEEE Workshop Color Photometric Methods Comput. Vis.*, 2003, pp. 1–8.
[13] Q. Zhu, J. Mai, and L. Shao, "A fast single image haze removal algorithm using color attenuation prior," *IEEE Trans. Image. Process*, vol. 24, no. 11, pp. 3522–3533, Nov. 2015.
[14] Y. Y. Schechner, S. G. Narasimhan, and S. K. Nayar, "Instant dehazing of images using polarization," in *Proc. Int. Conf. IEEE Comput. Vis. Pattern Recognit.*, 2001, pp. 325–332.
[15] Y. Y. Schechner, S. G. Narasimhan, and S. K. Nayar, "Polarization-based vision through haze," *Appl. Opt.*, vol. 42, no. 3, pp. 511–525, 2003.
[16] S. Shwartz, E. Namer, and Y. Y. Schechner, "Blind haze separation," in *Proc. Int. Conf. IEEE Comput. Vis. Pattern Recognit.*, New York, NY, USA, 2006, pp. 1984–1991.
[17] E. Namer, S. Shwartz, and Y. Y. Schechner, "Skyless polarimetric calibration and visibility enhancement," *Opt. Exp.*, vol. 17, no. 2, pp. 472–493, 2009.
[18] S. Fang, X. Xia, H. Xing, and C. Chen, "Image dehazing using polarization effects of objects and airlight," *Opt. Exp.*, vol. 22, no. 16, pp. 19523–19537, 2014.
[19] R. T. Tan, "Visibility in bad weather from a single image," in *Proc. Int. Conf. IEEE Comput. Vis. Pattern Recognit.*, Alaska, USA, 2008, pp. 1–8.
[20] R. Fattal, "Single image dehazing," *ACM Trans. Graph*, vol. 27, no. 3, pp. 1–9, 2008.
[21] J. P. Tarel and N. Hautiere, "Fast visibility restoration from a single color or gray level image," in *Proc. Int. Conf. IEEE Comput. Vis.*, Kyoto, Japan, 2009, pp. 2201–2208.
[22] J. H. Kim, W. D. Jang, J. Y. Sim, and C. S. Kim, "Optimized contrast enhancement for real-time image and video dehazing," *J. Vis. Commun. Image R*, vol. 24, no. 3, pp. 410–425, 2013.
[23] R. Luzón-González, J. L. Nieves, and J. Romero, "Recovering of weather degraded images based on RGB response ratio constancy," *Appl. Opt.*, vol. 54, no. 4, pp. 222–31, 2015.
[24] K. He, J. Sun, and X. Tang, "Single image haze removal using dark channel Prior," in *Proc. Int. Conf. IEEE Comput. Vis. Pattern Recognit.*, 2009, pp. 1956–1963.
[25] K. He, J. Sun, and X. Tang, "Guided image filtering," *IEEE Trans. Pattern Anal. Mach. Intell.*, vol. 35, no. 6, pp. 1397–1409, Jun. 2013.
[26] C. T. Chu and M. S. Lee, "A content-adaptive method for single image dehazing," *Lect. Notes Comput. Sci.*, vol. 6298, pp. 350–361, 2010.
[27] J. Yu and Q. Liao, "Fast single image fog removal using edge-preserving smoothing," in *Proc. Int. Conf. IEEE Acoust. Speech Signal Process.*, Prague, Czech Republic, 2011, pp. 1245–1248.
[28] C. H. Yeh, L. W. Kang, M. S. Lee, and C. Y. Lin, "Haze effect removal from image via haze density estimation in optical model," *Opt. Exp.*, vol. 21, no. 22, pp. 27127–27141, 2013.
[29] P. Carr and R. Hartley, "Improved single image dehazing using geometry," in *Proc. Int. Conf. Digital Image Comput., Tech. Appl.*, 2009, pp. 103–110.
[30] L. Schaul, C. Fredembach, and S. Süsstrunk, "Color image dehazing using the nearinfrared," in *Proc. Int. Conf. IEEE Image Process.*, 2009, pp. 1629–1632.
[31] X. M. Dong, X. Y. Hu, S. L. Peng, and D. C. Wang, "Single color image dehazing using sparse priors," in *Proc. Int. Conf. IEEE Image Process.*, 2010, pp. 3593–3596.
[32] S. G. Narasimhan and S. K. Nayar, "Vision and the atmosphere," *Int. J. Comput. Vis.*, vol. 48, no. 3, pp. 233–254, 2002.
[33] E. J. McCartney, "*Optics of the Atmosphere: Scattering by Molecules and Particles*," New York, NY, USA: Wiley, 1975.
[34] S. G. Narasimhan and S. K. Nayar, "Contrast restoration of weather degraded images," *IEEE Trans. Pattern Anal. Mach. Intell.*, vol. 25, no. 6, pp. 713–724, Jun. 2003.
[35] A. Levin, D. Lischinski, and Y. Weiss, "A closed form solution to natural image matting," in *Proc. Int. Conf. IEEE Comput. Vis. Pattern Recognit.*, New York, NY, USA, 2006, pp. 61–68.